INCEEUROPE

10th International Conference
on
Wind Turbine Noise
Dublin – 21st to 23rd June 2023

Wind turbine noise code benchmark: A comparison and verification exercise

Franck Bertagnolio¶, Andreas Fischer
DTU Wind and Energy Systems, Roskilde, Denmark

Christina Appel, Michaela Herr
DLR, Institut für Aerodynamik und Strömungstechnik, Braunschweig, Germany

Ferdinand Seel, Thorsten Lutz
Institut für Aerodynamik und Gasdynamik, Universität Stuttgart, Stuttgart, Germany

Koen Boorsma, Gerard Schepers, Miguel Restrepo Botero
Wind Energy, TNO Energy Transition, Petten, The Netherlands

Damiano Casalino, Wouter van der Velden
Dassault Systèmes Deutschland GmbH, Stuttgart, Germany

Carlo R. Sucameli
Lehrstuhl für Windenergie, Technische Universität München, München, Germany

Pietro Bortolotti
National Wind Technology Center, National Renewable Energy Laboratory, Golden, CO, USA

Summary

In a number of institutions and companies, researchers and engineers are developing numerical models and frameworks that are used to predict the aerodynamic noise emissions from wind turbine rotors. The simulation codes range from empirically tuned engineering models to high-fidelity computational ones. Their common feature is the fact that they all specifically model the main aerodynamic noise mechanisms occurring at the rotating blades (namely, the turbulent boundary layer): trailing-edge and turbulent inflow noise. Nevertheless, different modelling techniques and implementations may generate different results, even when assessed on the same rotor design and operating conditions, which raises the question of the actual fidelity and reliability of these

¶Corresponding author: frba@dtu.dk

models. Trailing-edge noise is put at the forefront of the present study, as it is recognized to be the main source of audible noise from modern wind turbines.

The present benchmark aims at comparing the results from different modelling approaches and drawing some conclusions from these comparisons. This effort, denoted as Wind Turbine Noise Code benchmark, was initiated in 2019 as a joint activity between the IEA Wind Task 39 (Quiet Wind Turbine Technology) and Task 29 (Detailed Aerodynamics of Wind Turbines, now Task 47).

In addition to the investigation of the noise emissions themselves, the rotor aerodynamic characteristics are investigated, as they are the source of the noise generation mechanisms discussed herein.

A number of test cases are defined, and the aerodynamic and aeroacoustic predictions from the various models are compared. A fair agreement between the aerodynamic predictions is observed. There exist some discrepancies between the different noise prediction methods, but it is difficult to conclude if one methodology is better than another in order to design a wind turbine with noise as a constraint.

1. Introduction

It is a well-accepted fact that trailing-edge (TE) noise is the prominent source of aerodynamic broadband noise from wind turbines in the audible range [35]. Therefore, it is important for the wind industry to assess and subsequently mitigate (e.g. using serration) this particular source of noise in order to reduce the environmental impact of wind turbines and wind farms. Aerodynamic noise sources also include turbulent inflow (TI) noise, which is normally more dominant at lower frequencies than TE noise (at least for modern multimegawatt wind turbines), but it can also be audible.

The present work aims at comparing various simulation methods for predicting and quantifying these two main aerodynamic noise sources from wind turbines. Note that other noise sources such as mechanical/tonal noise, low-frequency tower-blade interaction, tip noise, etc., are not considered in the present study, although these can have a significant impact on the acoustic footprint of a wind turbine. In addition, atmospheric propagation effects (such as reflection, refraction, diffraction, and air absorption) are also neglected, despite their potential impact on the perceived noise at dwellings.

This work is conducted as part of the IEA Wind Technology Collaboration Programme. Various institutions from participating countries have contributed to the present comparisons by using their own simulation framework that can model wind turbine aerodynamic noise emissions. The goal is to compare the different methodologies and analyze the consistency (or the lack thereof) of the results when simulating the same rotor in the same operating conditions.

In the following, the context and objectives of the present study are discussed. The various modelling strategies that are used for the comparisons are reviewed. The first part of the study concentrates on the comparisons of the aerodynamic quantities that are essential for the prediction of wind turbine aerodynamically generated noise. Then, the actual noise predictions are considered, focusing on the relationship between the aerodynamic and acoustic results. The study is concluded with comparisons of some of the model results with actual field noise measurement data from a wind turbine.

2. Context and objectives

TE and TI noise are the respective results of the interaction of the airfoil boundary layer (BL) and atmospheric turbulence with the blades. A variety of numerical methods have been derived to model these phenomena, ranging from relatively simple empirical formulae to high-end computationally expensive simulation codes. In a long-term effort, various models for TE noise were investigated at the airfoil level in a series of comparison rounds as part of the Benchmark Problems for Airframe Noise Computation (BANC) [20, 21]. The present study attempts to compare a number of these models when considering a full wind turbine rotor, identify some potential pitfalls in this context, and possibly improve the use and prediction results of these methods in the future. For example, higher-fidelity models could be used to tune or improve lower-fidelity ones, which are more suited to the constraint of a rapid turnaround time typical of industrial design.

The first objective is to make sure that the underlying aerodynamic simulations of the rotor flow are sufficiently close to each other, so that the impact on noise predictions related to possible discrepancies in the aerodynamic input data is minimized. Therefore, the first part of the study concentrates on rotor aerodynamic characteristics.

The second objective is to compare acoustic results. An analysis is conducted in an attempt to identify 1) the reasons for discrepancies between similar methodologies if/when such discrepancies are observed and 2) trends between different modelling approaches, e.g. empirical vs. high-fidelity models.

3. Computational methods

The various computational frameworks used in the present article are described in this section. A rough categorization of the different methodologies is introduced here.

The *first* step in the prediction of aerodynamic noise from a turbine usually consists of calculating the aerodynamic flow field around the turbine's rotor. Two main methodologies can be applied here:

- The most popular engineering method for predicting a wind turbine rotor flow aerodynamic is the blade element momentum (BEM) method, originally derived by Glauert [18], which is based on mass and momentum conservation principles.
- The second option is to numerically solve the associated conservation equations (here, Navier-Stokes or Euler) using computational fluid dynamics (CFD). This is usually much more computationally expensive.

The *second* step consists of defining the TE noise modelling approach. Note that the prediction of this noise source from wind turbines requires detailed boundary layer characteristics along the blades, which are normally not provided by BEM methods.

Three approaches are generally adopted:

- *Empirical modelling:* in all cases, this amounts to using the well-known Brooks Pope Marcolini (BPM) model [10]. Note that this model can include various aerodynamic noise sources (e.g. tip noise, blunt TE noise), but only TE noise is considered here. The model is based on theoretical work for the scaling of TE noise and empirical fitting using a series of experiments on the NACA0012, during which aerodynamic and acoustic properties were measured.

- *Semi-empirical modelling:* the models are extensions of the original model named TNO * developed by Parchen [36]. The TNO TE noise model and its revised versions are a combination of Kraichnan theory for BL turbulence, including various assumptions for characterizing the turbulence, and a scattering model for the TE noise prediction using either Howe or Amiet theory. A flow solver (CFD or Xfoil) is typically used for determining the aerodynamic and turbulent flow inputs to the overall model. These methodologies will be denoted as semi-empirical or TNO-type models in the following.
- *High-fidelity modelling:* the models are based on high-performance computing for solving the main rotor flow field and the acoustic field, either jointly or separately.

In addition, each of the above methods uses a flow solver to compute the aerodynamics around the blades, which are in most cases used as inputs for the above noise models (except when the aerodynamic and acoustic calculations are coupled, e.g. for the Lattice-Boltzmann Method).

Furthermore, as far as TI noise modelling is concerned, the frameworks used by the participants of the present comparison exercise are all implementations of the Amiet TI model [1, 37]. Two main versions can be distinguished here. The first one is the complete model implementation that involves the computation of the unsteady lift from a flat plate. The second is based on its asymptotic approximation for higher frequencies. Note that a simpler version using Lowson's method can also be used for TI noise modelling [30]. Nevertheless, more elaborate modelling methods are available for predicting TI noise from wind turbines [26].

The various numerical frameworks from the different participating institutions are summarized below. For further details about these frameworks, the reader is referred to the IEA Wind Technology Collaboration Programme website and the report specifically related to the present work [4].

3.1. TNO - SILANT

The aeroacoustic calculation of TNO is divided into three programs: Blademode [7], RFOIL [28], and SILANT[33].

BladeMode is an in-house aeroelastic blade stability software using the BEM theory. It is used in a quasi-steady configuration for the present application. The resulting sectional angle of attack and Reynolds number distribution along the blade span are then used as input to the SILANT model. This program includes the noise calculation from turbulent TE noise and tip noise based on the BPM model [10] and TI noise using the model of Amiet [1] and Lowson [29]. The RFOIL2D panel code with interacting BL is used to provide the boundary layer displacement thickness at the TE of the airfoil sections along the blade. The data are stored as a look-up table for the SILANT model.

The resulting sectional noise source strengths are acoustically summed over the blades and rotor. In addition to calculating noise sources, SILANT can also include Doppler effects (and additional effects related to atmospheric propagation which are ignored in the present work).

3.2. NREL - OpenFAST

OpenFAST is a popular multi-physics solver developed and released by the National Renewable Energy Laboratory. OpenFAST integrates an aeroacoustic model that is described in Bortolotti et al. [8]. The model implements a conventional turbulent inflow model from Amiet [1], with the optional

*Note that the designation of the so-called TNO TE noise model originates from the institute where its conceptor worked at the time. It is the same TNO institute at which two of the authors of the present article are working. In order to avoid confusion, it must be made clear that these two authors use a different TE noise model in their computational framework, but that both models will be referred to as TNO in the figure captions.

correction defined by Moriarty et al. [34]. The model also implements the noise sources defined by Brooks et al. [10]. The models implemented in OpenFAST were subjected to a validation study operating a GE 1.5 MW wind turbine. The results are discussed in Bortolotti et al. [9] and Hamilton et al. [19].

3.3. TUM - Cp-Max AAM

This framework is the one described in [41]. It is based on the in-house-developed aeroservoelastic wind turbine solver Cp-Lambda, which implements a BEM formulation and provides the aerodynamic inputs necessary for the aeroacoustic calculations.

Several aeroacoustic models are implemented within this framework. For the purpose of the present paper, TE noise results are provided for two different models (the BPM model [10] and a version of the TNO model described in [41]). For both models, 2D boundary layer characteristics are obtained through XFoil. TI noise spectra are provided for two different formulations of the Amiet model. The first formulation is the full implementation of [37], while the second one corresponds to the approximations of the Amiet model for high and low frequencies. An additional low-frequency correction is included, as shown in [30].

3.4. IAG Stuttgart - IAGNoise+

The Institute of Aerodynamics and Gas Dynamics (University of Stuttgart, Germany) uses the IAGNoise+ noise prediction code. This semi-empirical model computes the generated TE noise based on 3D flow solutions from CFD simulations. In this work, Reynolds-averaged Navier Stokes (RANS) simulations using a k-ω SST turbulence model were run with the flow solver FLOWer.

IAGNoise+ employs a TNO-Blake-type model for the computation of TE noise [5]. Compared to a classical TNO-type model, the current implementation [22] includes the part of the wall pressure fluctuation source term that is associated with turbulence-turbulence interaction and usually neglected in the basic model. This inclusion allows for more accurate predictions at higher angles of attack, where slight to moderate flow separation occurs. Additionally, the anisotropy factor was adjusted to also include adverse pressure gradient effects. The IAGNoise+ prediction tool also offers a way to calculate inflow noise, based on the model proposed by Paterson and Amiet [38] with Moriarty's thickness correction [34].

3.5. DTU - HAWC2-Noise

This framework uses the HAWC2 code [27] as a basis. It is a time-domain multibody aeroelastic code used for the study and design of wind turbines. The blade element momentum theory by Glauert [18] is applied in order to calculate the aerodynamic loading [32].

The aerodynamic data are used as inputs to an acoustic module that can account for TI noise using the Amiet model [1], and TE noise using a version of the TNO model [17] for which scattering is accounted for using the Amiet model [2]. Both noise model formulations are in the spectral domain. Therefore, it is assumed that that the acoustic emissions are quasi-stationary (at each time step of the aeroelastic solver), and spectrograms can be obtained for each of the noise sources. The detailed aerodynamic characteristics of the turbulent BL, which are used as input to the TE noise model, are computed as a preprocessing step with the 2D RANS solver EllipSys2D at each discrete section along the blades.

3.6. 3DS wind turbine multi-fidelity approach

Wind turbine aerodynamic and acoustic calculations have been performed using the multi-fidelity framework *Opty∂B*-WTNOISE® [12, 42]. Three approaches have been used: one is based on a blade element momentum theory (BEMT) rotor aerodynamic calculation, and the other two rely on lattice Boltzmann method very large eddy simulation (LBM-VLES) scale-resolved transient flow simulations.

3.6.1. BEM-based methodology

The BEMT tool uses BEM theory with uniform inflow and tip-loss correction [11], and a viscous panel method available in *Opty∂B*-BEMT is used for defining the boundary layer flow on the blades [13, 14]. Wall pressure spectra are computed with semi-empirical formulations. On the suction side, a model is used, obtained by blending Schlinker's [40] model at low frequency with Kamruzzaman's [25] model at high frequency, and by recalibrating the overall energy to the Schlinker model value. On the pressure side, the Schlinker model is used. The Schlinker and Amiet model is used for TI noise [1].

3.6.2. 2.5D LBM/FW-H-based methodology

PowerFLOW® 2.5D simulations are performed by means of a fully automatic workflow fed with sectional coordinate profiles generated by *Opty∂B*-PFROTOR, and values of Mach number and angle of attack computed by *Opty∂B*-BEMT [12].

Simulations are carried out on extruded blade sections of fixed span of 0.1 m. For every radial strip selected by the user from the available blade segmentation, the PowerFLOW simulation generates a transient wall pressure file which is used by the frequency-domain FW-H solver *Opty∂B*-FWHFREQ executed by *Opty∂B*-WTNOISE. Full-blade noise spectra are recovered by *Opty∂B*-WTNOISE via an incoherent summation of sectional noise spectra, scaled by the ratio of the physical spanwise extension of the blade strip and the 2.5D simulated span.

3.6.3. 3D LBM/FW-H-based methodology

PowerFLOW 3D simulations are performed by means of a fully automatic workflow used for multicopter eVTOL, rotorcraft, fan, and wind turbine applications [12]. A series of simulations are carried out with mesh refinement in different blade strips where the turbulent scales are trigged by a trip. Similar to the 2.5D approach, the full turbine noise levels are recovered by incoherent summation of the individual strip contributions.

3.7. DLR - hybrid RANS-based CAA method PIANO/FRPM

An automatized 2D process chain for turbulent boundary layer trailing edge noise (TBL-TEN) [16, 39] is used to provide an acoustic prediction for trailing-edge noise of 2D profiles. Originally developed to assist low-noise airfoil design optimization, this method has been validated in detail within the BANC framework [20, 21]. The process chain operates via bash scripting the input parameters (like airfoil geometry, Reynolds number, angle of attack, chord length and process parameters, e.g. number of iterations, simulated real time and post processing options). The CFD code TAU, which is developed at the German Aerospace Center (DLR), is applied for the RANS simulations, and the DLR computational aeroacousics (CAA) code PIANO with the stochastic sound source model FRPM [15] (**F**ast **R**andom **P**article **M**esh method) is applied for the acoustic prediction.

In a second step, the results from the process chain are combined with DLR's TAP (**T**urbine **A**coustic **P**rediction) tool to extrapolate and summarize the data for a complete rotor [3]. Ongoing work includes the successive extension of TAP by additional semi-empirical source models for flow separation and TI noise. TI noise predictions applied herein are based on Hornung et al. [23].

4. Test case definitions and physical inputs

All the calculations presented in this article are based on the 2.3 MW wind turbine NM80. The use of the NM80 turbine geometry has been granted to the participants of Task 39 for the present study. This turbine was initially investigated as part of the DANAERO project [31]. It was further used as a reference turbine for the aerodynamic benchmark that was conducted as part of IEA Wind Task 29 (now Task 47) [6]. Some details of the turbine geometry can be found in the latter publications. Four test cases were defined for the present study, although only one of them will be considered in the present article. The main operational conditions of interest are the following:

- Test Case 1.1: Axisymmetric configuration (i.e. no rotor tilt), rigid structure, a wind speed of 6.1 m/s, turbulence intensity of 8.96%, and a rotor speed of 12.3 rpm. Additional information such as atmospheric conditions, blade pitch, etc., are also specified.

For the rotor noise calculations, a number of observer positions are defined. Twelve positions are defined on the ground around the turbine, equally distributed on a circle with a radius equal to the maximum height of the turbine (i.e. tower height plus half-rotor diameter), as depicted in Fig. 1. In addition, a single point is located at the same distance but on the rotor axis in the downstream direction. Note that in all noise calculations, atmospheric propagation effects and ground reflections are discarded, but the geometrical spreading is accounted for.

In addition, results from a noise measurement campaign conducted on a megawatt-size turbine will be considered.

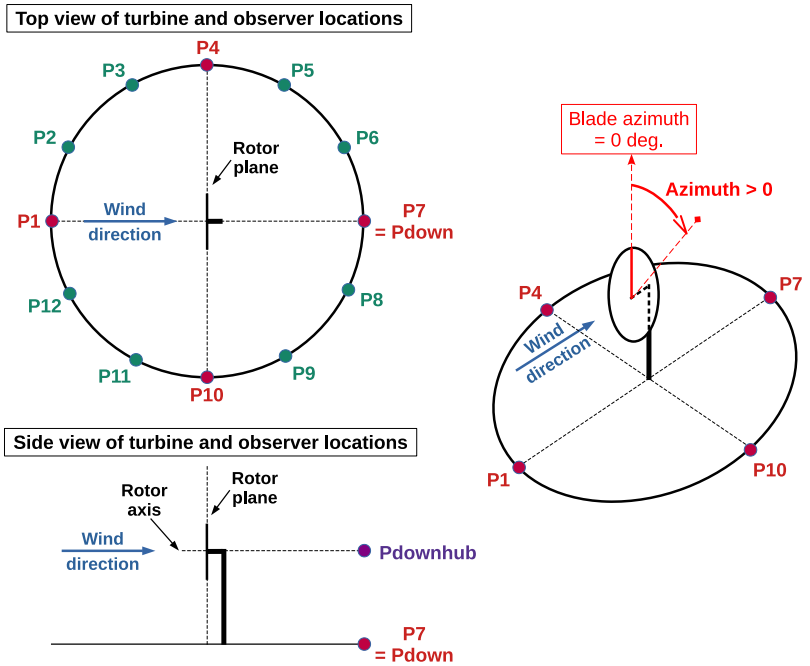

Fig. 1 Sketch of the observer locations around the turbine for the noise calculation results.

5. Comparison of aerodynamic results

As mentioned earlier, the aeroacoustic emissions of a wind turbine are highly dependent on the atmospheric inflow and resulting flow on the blades, which is computed using BEM theory or CFD in this work. Therefore, the first step for comparing numerical frameworks is comparing the aerodynamic data along the blades. Three spanwise locations along the blades were chosen for the comparisons: $r = 19$ m, 30 m and 37 m from the root of the blade.

Note that since both TI and TE noise are scaling with the Mach number (to a specific power depending on the mechanism), it is well-known that toward the blade tip, as the effective velocity becomes higher, the aerodynamic noise emissions increase. Consequently, this study focuses on BL characteristics on the outer part of the blades.

5.1. Incoming flow

The relative and effective (i.e. including rotor induction) inflow velocities, angles of attack, and lift and drag coefficients at the three spanwise locations are displayed in Fig. 2. The agreement between the inflow velocities is nearly perfect, which is consistent with the imposed rotor speed of the test case. Some discrepancies are observed between the calculated angles of attack, but these remain relatively small, within less than 1 deg, and these appear to become even smaller toward the tip of the blade. The lift coefficients present very small discrepancies as well, but the drag coefficients do depart more significantly.

Overall, all methods deliver similar results in terms of the aerodynamic loading on the turbine.

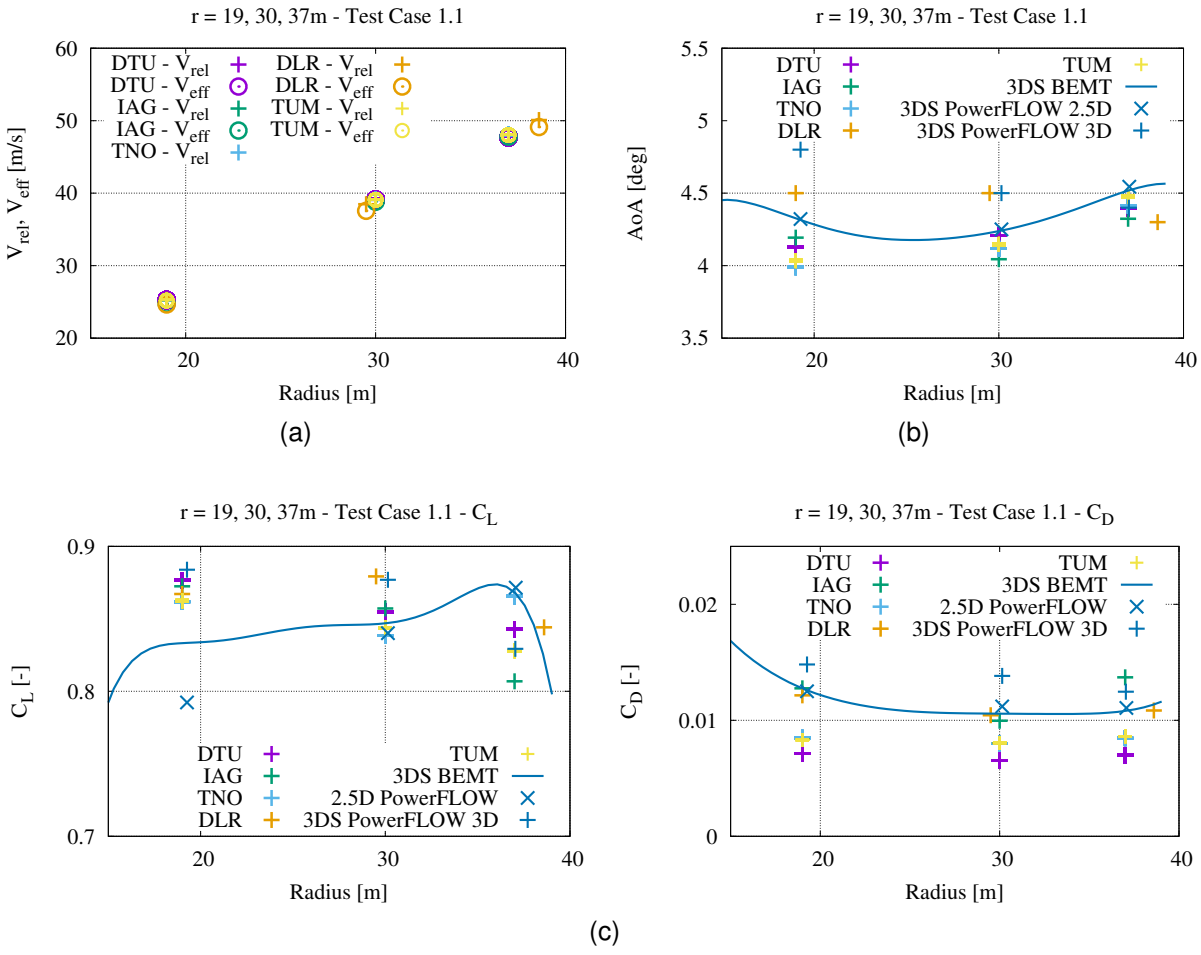

Fig. 2 Aerodynamic quantities of the incoming flow along the blade span: (a) relative and effective inflow velocity, (b) angle of attack, and (c) lift and drag coefficients.

5.2. Boundary layer thicknesses and profiles near the TE

It is well-known that the turbulent BL characteristics near the TE have a large impact on the TE noise emissions. These characteristics are investigated in the present section.

The BL thickness δ, BL displacement thickness δ^*, and BL momentum thickness θ are displayed in Fig. 3 for the suction and pressure sides. It can be observed that there is relatively good agreement between all methods, and that the discrepancies appear to be getting smaller toward the tip of the airfoil, which should contribute to a better convergence of the aerodynamic noise model results in the following sections.

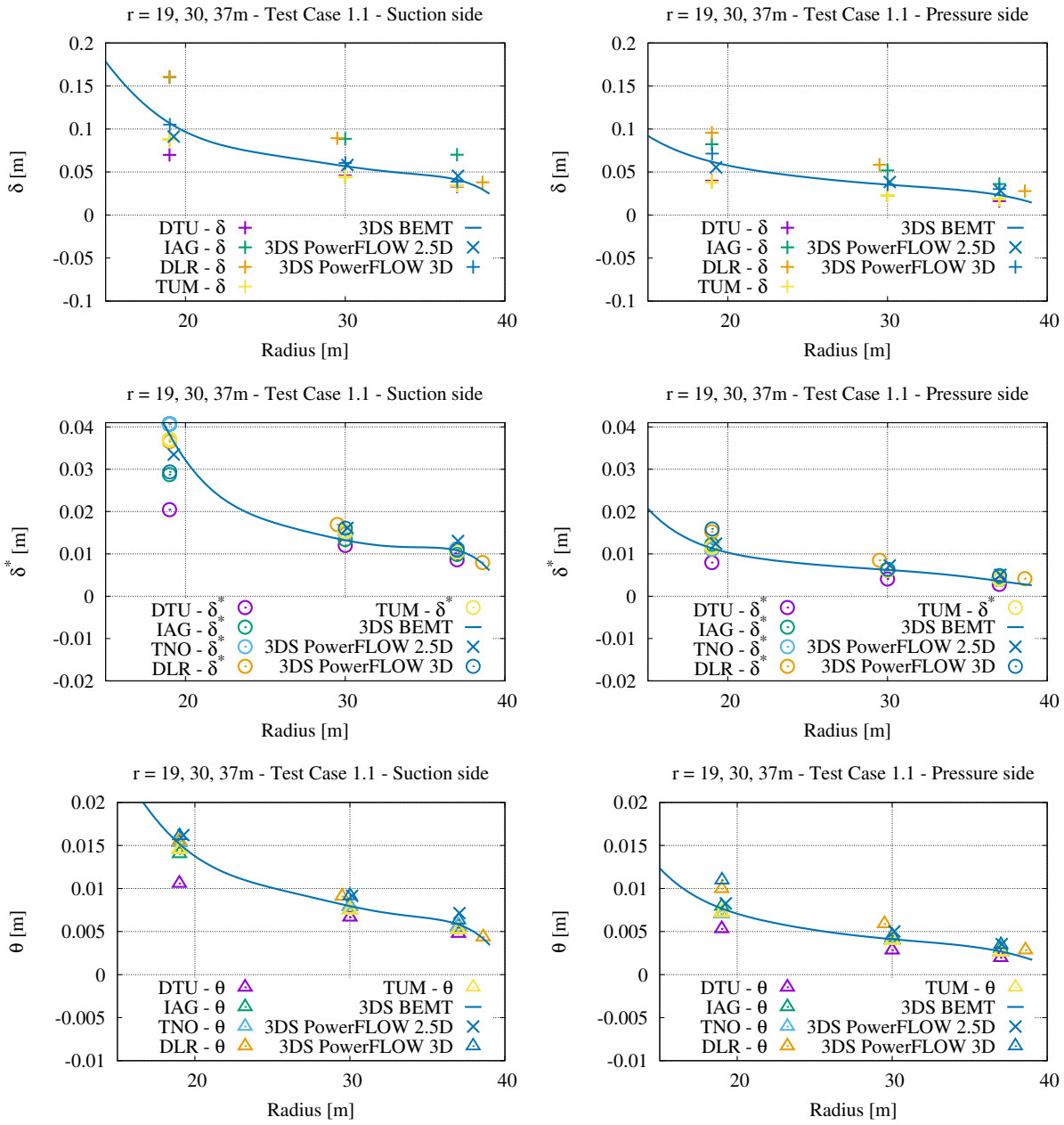

Fig. 3 Boundary layer thickness (top), displacement thickness (middle), and momentum thickness (bottom) along the blade span on the *suction* side of the airfoil at $x/C = 93\%$ (left) and *pressure* side at $x/C = 91\%$ (right).

The boundary layer profiles for BL velocity, turbulent kinetic energy, turbulence dissipation rate, and

integral length scales, which are again important parameters influencing TE noise, are displayed in Fig. 4 for the suction and pressure sides at the outer spanwise section $r = 37$ m. Note that results from only a few methods are displayed here, as these quantities do not need to be explicitly calculated in some of the present numerical frameworks in order to compute TE noise.

There are noticeable discrepancies in the turbulent quantities. Note here that DLR and the Technical University of Denmark (DTU) use 2D CFD calculations to obtain the BL profiles at various sections along the span, whereas the University of Stuttgart Institute for Aerodynamic and Gas Dynamics (IAG) conducts a full 3D CFD simulation of the entire blade. This may affect the resulting computed BL profiles.

The impact of these turbulent BL quantities on the surface pressure spectra at the same location (see Section 5.3), and TE noise at the rotor level (see Section 6), is investigated in the following.

5.3. Surface pressure spectra near TE

The surface pressure spectra on the suction side at $x/C = 93\%$ and pressure side at $x/C = 91\%$ (i.e. relatively close to the TE) are displayed in Fig. 5. Since these spectra are characteristics of the turbulent flow in the vicinity of the TE, it is expected that they will have a large impact on the TE noise emission.

There is relatively good agreement between DTU, IAG, and the 3DS BEMT results above the peak frequency around 400–500 Hz on the suction side. The 3DS PowerFLOW results show higher spectral levels across the whole frequency range with slightly smaller slope above the peak frequency. It is noteworthy that all methods exhibit peak frequencies close to each other.

However, the discrepancies are larger on the pressure side. Nevertheless, all methods exhibit higher peak frequencies, which could be expected from the smaller BL thicknesses (see Fig. 3) and lower integral length scales (see Fig. 4). The spectra appear flatter above peak frequency for most methods. In addition, the spectral levels, e.g. at peak frequencies, are also lower in agreement with the observed lower turbulent kinetic energy levels on the pressure side (see Fig. 4).

When comparing high-fidelity model results to those that use the semi-empirical TNO model (or its variants) in Fig. 6, it is observed that the high-fidelity results (here, only PowerFLOW 2.5D and 3D) indicate a larger energy content in the low-frequency range, but also at high frequencies for the suction side. The semi-empirical methods also appear to converge on the suction side at higher frequencies.

The main takeaway from the present section is a lack of variety of methodologies for evaluating the surface pressure, which prevents the drawing of firmer conclusions. It is restricted here to three semi-empirical modelling approaches, with the LBM approach being the only one characterized by high modeling fidelity. Since surface pressure is the direct link between the boundary layer turbulent quantities and the noise emission, this is probably key to a better understanding of the discrepancies between the different noise models at the rotor level.

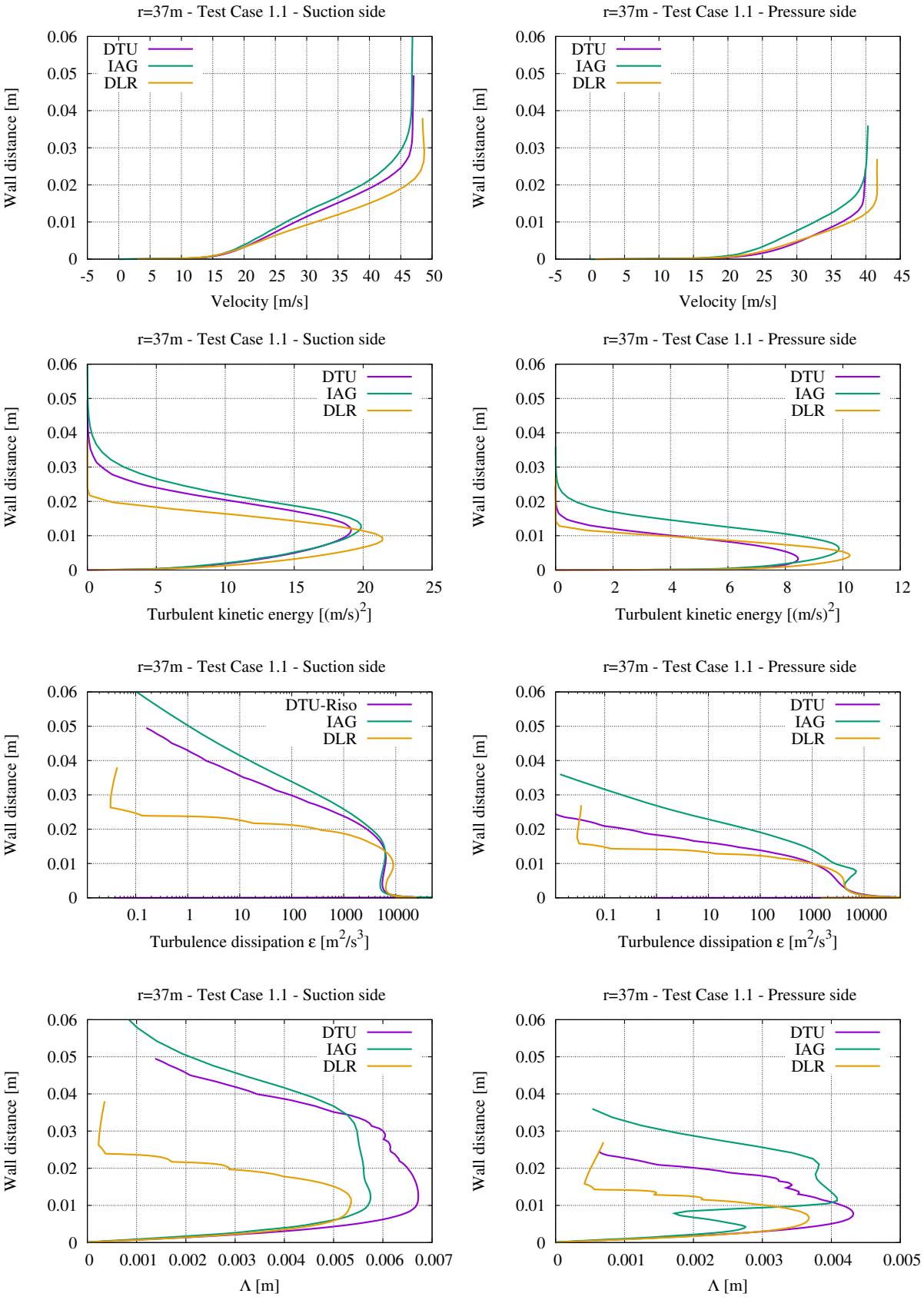

Fig. 4 Boundary layer profiles of: velocity (top row), turbulent kinetic energy (second row), turbulence dissipation rate (third row), and integral length scale (bottom row) at the blade span $r = 37$ m on the suction side of the airfoil at $x/C = 93\%$ (left) and pressure side at $x/C = 91\%$ (right).

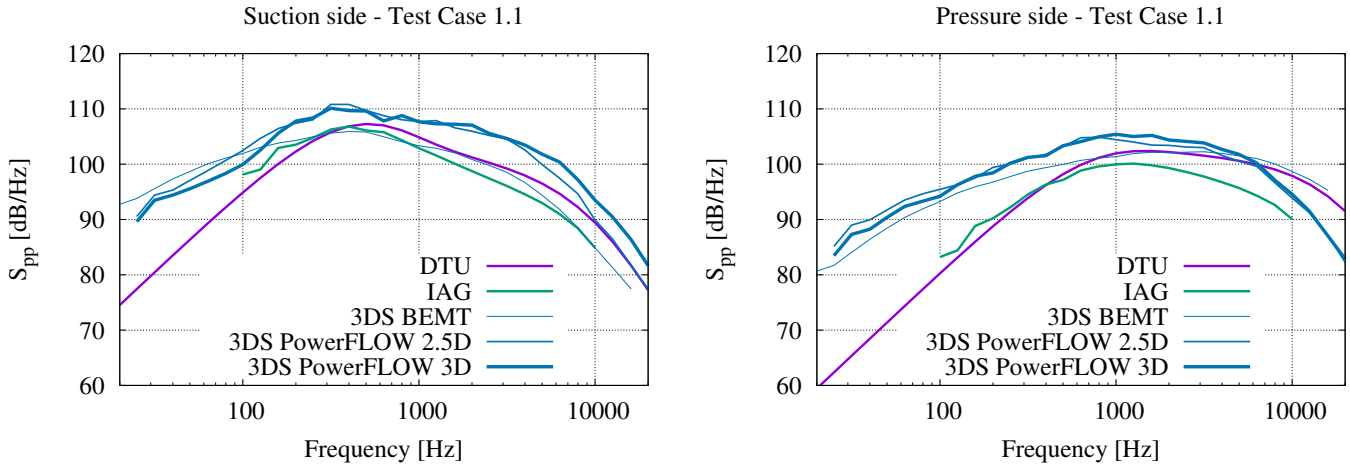

Fig. 5 Surface pressure spectra on the suction side at $x/C = 93\%$ (left) and on the pressure side at $x/C = 91\%$ (right) at the blade span $r = 37$ m.

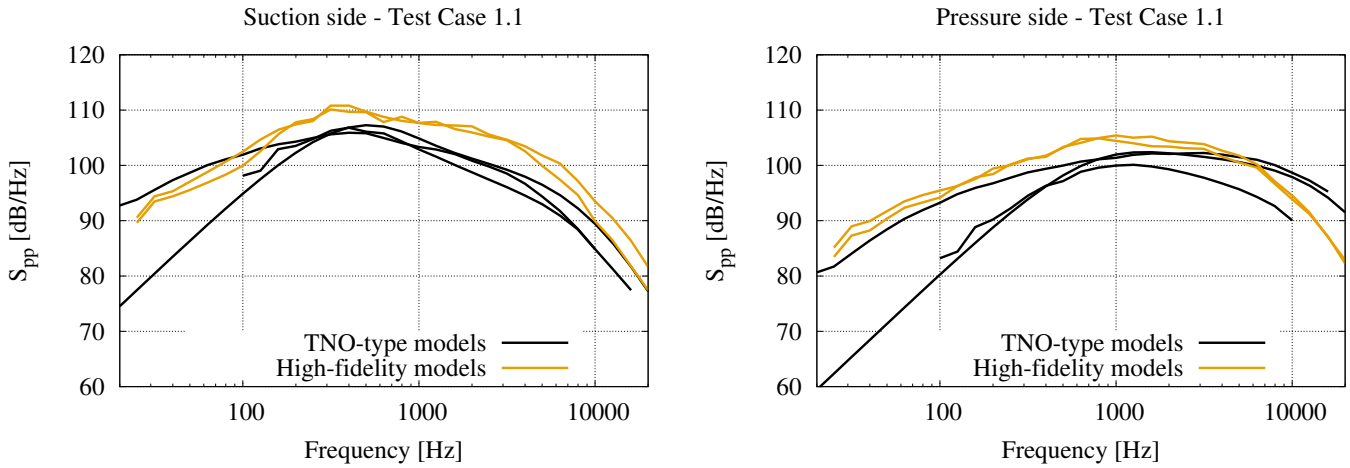

Fig. 6 Surface pressure spectra on the suction side at $x/C = 93\%$ (left) and on the pressure side at $x/C = 91\%$ (right) at the blade span $r = 37$ m.

6. Comparison of acoustic results

In this section, the aerodynamic noise emission of the full rotor is discussed.

6.1. Test case 1.1

The individual contributions from the TI and TE noise at the ground location downstream of the turbine are displayed in Fig. 7.

There is good agreement in the TI noise predictions in the high-frequency range, for $f \gtrsim 200$ Hz. This is to be expected for two separate reasons: first, all implementations are essentially similar, since they are based on the same Amiet model. Second, the model is built for a flat plate at no incidence. It follows that the actual blade shape or its angle of attack distribution does not influence the output of TI models and is mainly influenced by the velocity distribution along the blades, which is essentially identical for all the frameworks considered.

Below 200 Hz, two groups of prediction methods emerge: one predicts a continuous spectral slope toward lower frequencies while the other exhibits a higher energy bump in this frequency range. From Fig. 8, it is clear that the difference lies in the implementation of the full Amiet TI model, or its high-frequency asymptotic approximation, as discussed in Section 3. In addition, there is a larger spread of the results for the full Amiet models, which is attributed to the various implementations by the different participants. This highlights the dependency of rotor noise on the specific airfoil noise models, and this would probably require further investigations at the airfoil level.

Regarding TE noise, the spread of the model results is larger than for TI noise, as expected. The spectral slopes of the different models in the high-frequency range appear in good agreement, although an energetic spread with an amplitude slightly lower than 10 dB exists at any given high frequency. Looking toward the spectral peak, the peak frequency is in relative good agreement for all methods, with a spread amplitude of approximately 200 to 300 Hz. However, there is an even larger spread in the peak spectrum values. It is noteworthy that the high-fidelity methods, which exhibited larger energy levels for the wall-pressure spectra (see Section 5.3), now predict lower noise levels.

Looking at TE noise in Fig. 8, a number of features emerge that distinguish between high-fidelity, semi-empirical (TNO-type) and empirical (BPM) models, as discussed in Section 3. High-fidelity models predict lower spectral energy in the high-frequency range (beyond peak frequency), although a more noticeable energy bump at higher frequencies (above 1000 Hz) emerges. The latter is probably caused by the pressure-side TE noise contribution, since bluntness noise is not included in these models. This spectral bump is not clearly visible in the other modelling approaches, if it is indeed caused by the pressure-side TE noise contribution, even though it is a part of them. The trends for the different high-fidelity models are different for the low-frequency range. The empirical models consistently predict higher energy levels in the high-frequency range. The semi-empirical models lie somewhere in between for most of the spectral range, with some of them predicting lower energy for the pressure-side spectral bump at very high frequency.

The above comparisons, in particular for TE noise, indicate that there is a need to simplify the comparisons in order to trace back the origin of the observed discrepancies at the rotor level. It could be implemented by coming back to a simpler configuration with a rotating airfoil section of limited span [4], or even to a static 2D airfoil [20, 21] for which comparisons with wind tunnel data are possible.

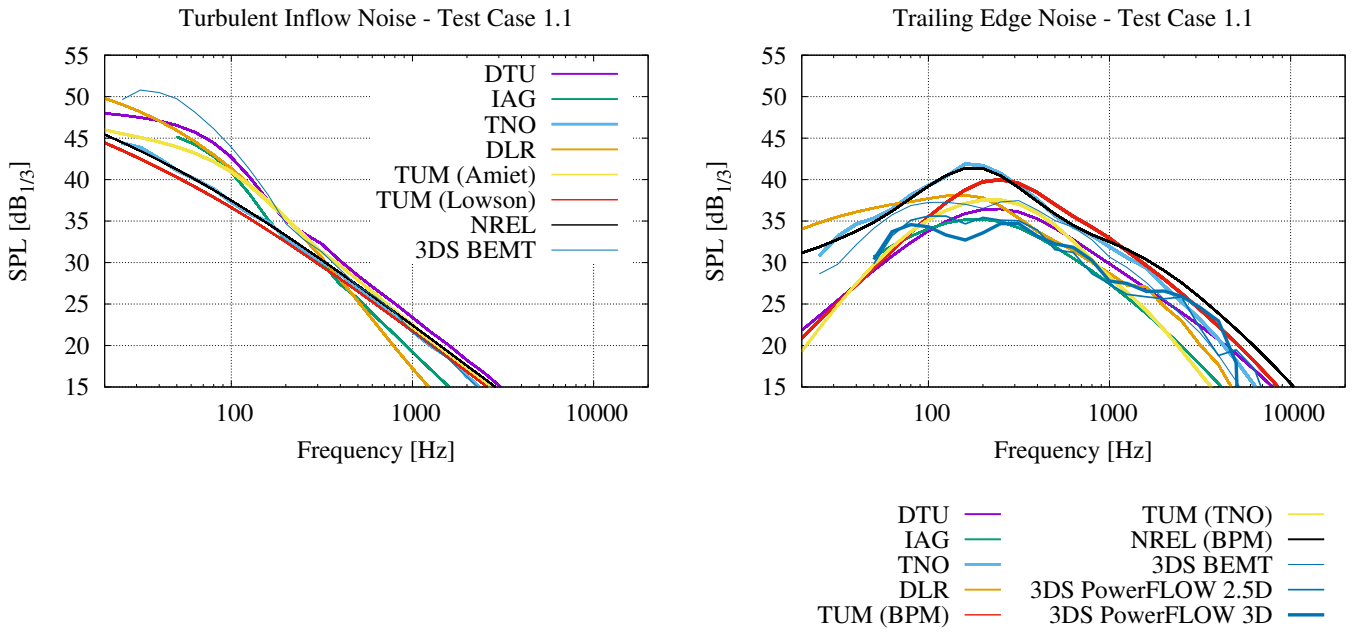

Fig. 7 TI noise (left) and TE noise (right) spectra at a location downstream of the rotor on the ground.

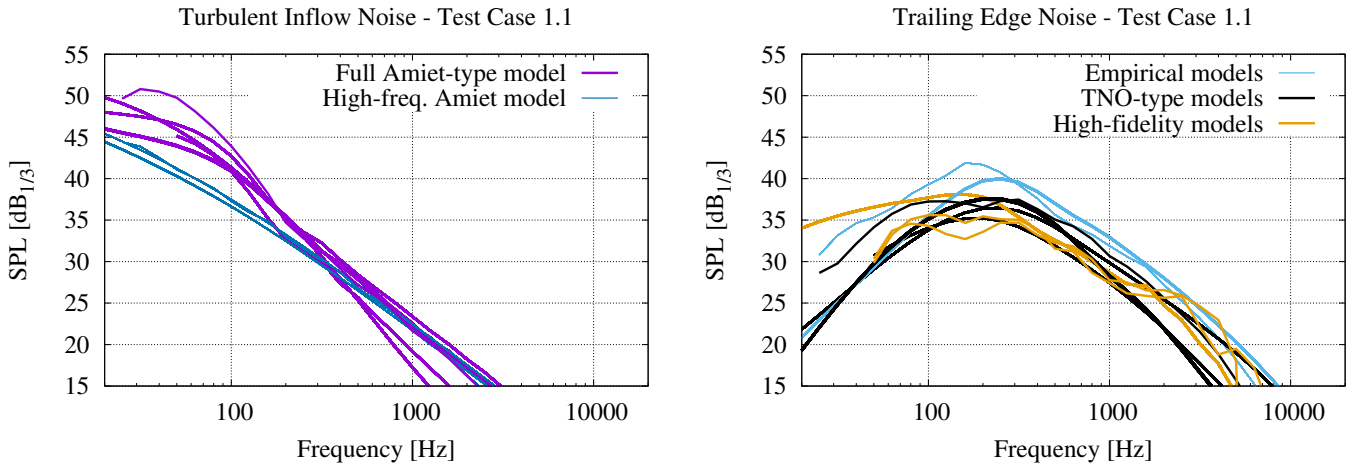

Fig. 8 TI noise (left) and TE noise (right) spectra at a location downstream of the rotor on the ground.

6.2. Wind turbine noise model directivity pattern

Test-case 1.1 is also used to investigate the directivity pattern around the wind turbine on the ground. As mentioned earlier, the noise spectra are predicted at various locations distributed around the turbine. These spectra are A-weighted and integrated across frequency and displayed in Fig. 9.

All models predict a reduction of noise in the plane of the rotor, although with various amplitudes relative to the upstream and downstream directions. This is an expected result given the more dipole-like behavior of TI noise, explaining the sharper deficit observed in the figure for this specific noise mechanism. The cardioid directivity pattern for TE noise, at airfoil level, similarly leads to a rotor plane noise deficit, which appears less pronounced.

Furthermore, the directivity pattern appears symmetric with respect to the rotor plane. Common sense would suggest that the perceived noise is higher downstream of the rotor, but it must be reminded that atmospheric effects are not included here.

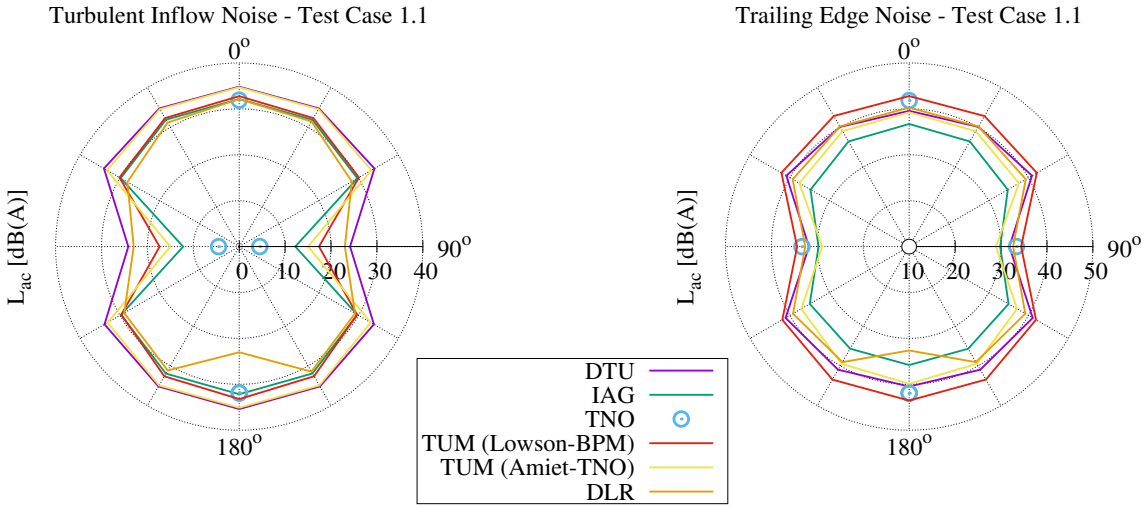

Fig. 9 A-weighted integrated spectra of TI noise (left) and TE noise (right) around the turbine on the ground.

6.3. Comparison with noise field measurements

The measurement of wind turbine noise for site assessment is often conducted according to the IEC 61400-11 standard [24]. The NM80 turbine that has been considered in the present work has been acoustically assessed using that standard. In the present section, the model results are compared to these field noise measurements.

The measured noise spectrum at a wind speed of 8 m/s is compared with six different models in Fig. 10. Note that the TI contribution for the DLR results is an extrapolation of lower wind speed data, and that it might slightly underestimate the actual noise level in the frequency range 100–400 Hz, but the results are unaffected above peak frequency at 500 Hz.

A higher energy spectral bump is observed in the measurements in the frequencies ranging from 100 to 300 Hz. It is attributed to mechanical noise, as a spectral tone at the center frequency of 137 Hz has been clearly identified during the same measurement campaign. This is compatible with the observed local energy peaks maxima located at the 1/3 octave band center frequencies: 125 Hz for the fundamental tone and 250 Hz and 500 Hz for the harmonics. Therefore, the models

that do not account for mechanical noise are underpredicting the measurement data in this frequency range. Elsewhere there is a good agreement between models and measurements, which stay nearly within the ±2 dB uncertainty margin of the measurements, except at very low and very high frequencies. As expected from the results observed in the previous section, the Lowson-TNO approach underpredicts the noise levels in the low-frequency range corresponding to the TI noise contribution, and overpredicts in the high-frequency range where TE noise dominates.

The acoustic power curves of the A-weighted integrated spectra as a function of wind speed are displayed in Fig. 11. The model results remain again within ±2 dB of the measured noise levels, except at the wind speed of 6 m/s. Unfortunately, the measured spectrum is not available at this wind speed. The reason for this discrepancy remains unknown. It was checked that the design rotational speed and blade pitch at this wind speed did match the design electrical power output in the HAWC2 model. Therefore, it can only be surmised that the turbine controller is more aggressive/optimal than the design parameters available for the present comparisons, and that rotational speed is increased at this particular wind speed in reality to maximize the power output.

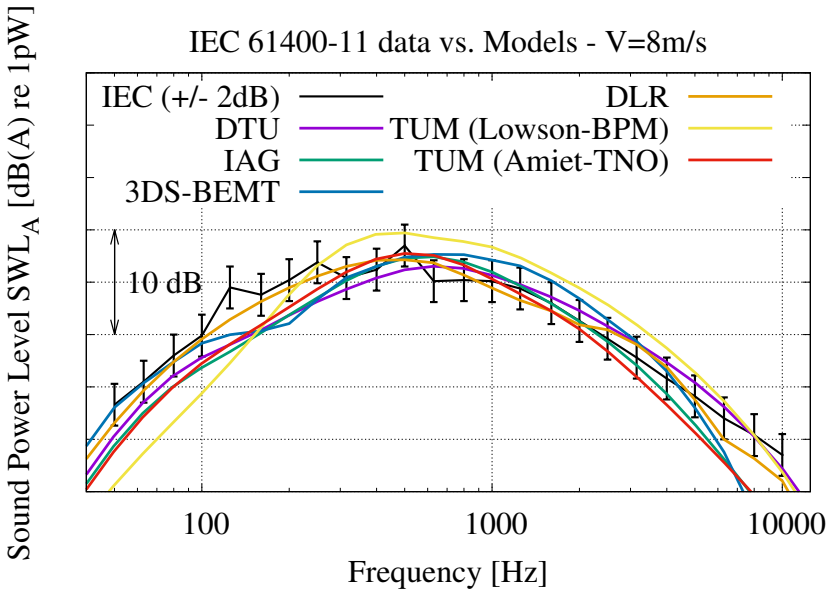

Fig. 10 A-weighted sound power spectrum of the measured noise using IEC 61400-11 standard measurement procedure versus model results for a wind speed of 8 m/s.

7. Conclusions

The comparisons presented in this paper highlight a number of discrepancies when evaluating wind turbine rotor noise with various methodologies based on airfoil TI and TE noise modelling.

It is observed that the use of a single identical model for TI noise (Amiet model) and its different implementations may yield significantly different noise predictions at the rotor level. Nevertheless, this model appears to be the main engineering approach for modelling this phenomenon, although higher-fidelity models exist.

Regarding the prediction of TE noise and the analysis conducted in the present work, a bottleneck is identified. It resides in connecting the aerodynamic quantities, in particular the turbulent

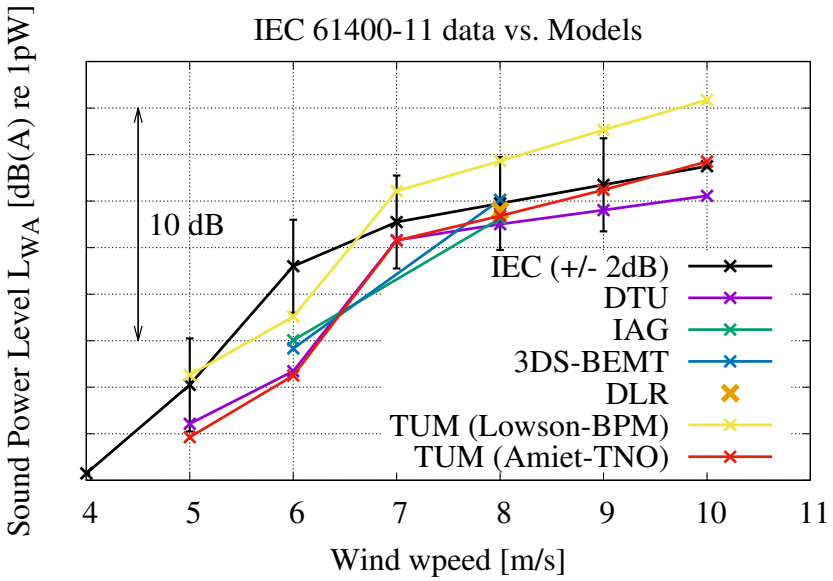

Fig. 11 Integrated A-weighted sound power as a function of wind speed using IEC 61300-11 standard measurement procedure versus model results.

boundary layer, to the rotor noise emission through the surface pressure. Indeed, the surface pressure models have not been thoroughly investigated, mainly because of a lack of available results. The use of simpler configurations is therefore suggested, e.g. limited spanwise section, or even 2D section in standstill, in order to identify the origin of these discrepancies.

A largely expected result from the present study is the presence of a noise level deficit in the rotor plane. This feature has been observed earlier in the field as well as in numerical predictions. The present contribution tends to confirm that there is a sharper deficit originating from TI noise, which would suggest that it is even more pronounced at lower frequencies.

Note that wind turbine designers in the industry, while mostly resorting to empirical models in the design loops for reducing turnover time, have access to a considerable amount of experimental data which can be used to tune and improve their modelling frameworks. The present study indicates that introducing semi-empirical models, which aim at accounting for more physical processes in the prediction tools, still suffer from relatively large discrepancies between each other when predicting rotor noise emissions. Therefore, it can be surmised that tuning or improving these models is still required. High-fidelity model results appear to somehow converge for TE noise within the high-frequency range, still with some discrepancies. Note, however, that only two high-fidelity approaches (for TE noise) were considered in the present work. Nevertheless, when comparing different models of varying fidelity with actual wind turbine noise measurements, it appears that all model results stay for the most part within the ± 2 dB uncertainty margin associated with the field measurement.

To conclude, real field conditions are difficult to reproduce within rotor noise models (e.g. blade leading edge erosion or fouling, atmospheric turbulence influencing the BL turbulence and subsequently TE noise, etc.). These are also difficult to identify (when comparing with measurements) and quantify. Therefore, many aspects remain to be considered for developing accurate prediction models for wind turbine rotor noise.

Acknowledgments

The present benchmark is conducted as a sub-task of the IEA Wind TCP research Task 39 (Quiet Wind Turbine Technology), as well as a part of IEA Wind TCP research Task 29 Phase IV (Analysis of Aerodynamic Measurements).

DTU participation was partly supported by the EUDP projects Jr.nr. 64016-0056 and Jr.nr. 134-21022 funded by the Danish Energy Agency (Energistyrelsen), as well as by countries participating to the Task for supporting the Operating Agent duties.

The DanAero projects were funded partly by the Danish Energy Authorities (EFP2007. Journal nr.: 33033-0074 and EUDP 2009-II. Journal nr.: 64009-0258), and partly by eigenfunding from the project partners Vestas, Siemens, LM, Dong Energy and DTU.

Financial support of the German Federal Ministry for Economic Affairs and Climate Action (BMWK) to the operation of Task 39 is also highly acknowledged.

The authors are thankful to Vestas Wind Systems A/S for providing the noise measurements of the NM80 turbine, as well as allowing their anonymized display in the present article.

This work was authored in part by the National Renewable Energy Laboratory, operated by Alliance for Sustainable Energy, LLC, for the U.S. Department of Energy (DOE) under Contract No. DE-AC36-08GO28308. Funding provided by the U.S. Department of Energy Office of Energy Efficiency and Renewable Energy Wind Energy Technologies Office. The views expressed in the article do not necessarily represent the views of the DOE or the U.S. Government. The U.S. Government retains and the publisher, by accepting the article for publication, acknowledges that the U.S. Government retains a nonexclusive, paid-up, irrevocable, worldwide license to publish or reproduce the published form of this work, or allow others to do so, for U.S. Government purposes.

References

[1] Amiet, R. K. (1975). Acoustic Radiation from an Airfoil in a Turbulent Stream. *J. Sound Vib.*, 41(4):407–420.

[2] Amiet, R. K. (1976). Noise due to Turbulent Flow Past a Trailing Edge. *J. Sound Vib.*, 47(3):387–393.

[3] Appel, C., Faßmann, B., and Lin, S. (2020). CAA-basierte Schallvorhersage für Windkraftanlagen. In *DAGA 2020 (Conference)*, Hannover, Germany. Deutsche Gesellschaft für Akustik e.V.

[4] Bertagnolio, F., Fischer, A., Seel, F., Lutz, T., Hornung, C., Boorsma, K., Schepers, G., Botero, M. R., Appel, C., Herr, M., Sucameli, C., Bortolotti, P., v. d. Velden, W., and Casalino, D. (2023). Task 29 T3.7 & Task 39 Wind Turbine Noise Code Benchmark - Preliminary Results. Retrieved from: https://usercontent.one/wp/iea-wind.org/wp-content/uploads/2021/05/report_WTNCBenchmark.pdf, Accessed: 2023-04-29, IEA Wind TCP.

[5] Blake, W. K. (1986). *Mechanics of Flow-Induced Sound and Vibration, Vol.I and II*, volume in Applied Mathematics and Mechanics. Frenkiel, F.N. and Temple, G. (eds.), Academic Press.

[6] Boorsma, K., Schepers, G., Aagard Madsen, H., Pirrung, G., Sørensen, N., Bangga, G., Imiela, M., Grinderslev, C., Meyer Forsting, A., Shen, W. Z., Croce, A., Cacciola, S., Schaffarczyk, A. P., Lobo, B., Blondel, F., Gilbert, P., Boisard, R., Höning, L., Greco, L., Testa, C., Branlard, E., Jonkman, J., and Vijayakumar, G. (2023). Progress in the validation of rotor aerodynamic codes using field data. *Wind Energy Science*, 8(2):211–230.

[7] Boorsma, K. and Schepers, J. (2011). Enhanced wind turbine noise prediction tool SILANT. In *Presented at the Fourth International Meeting on Wind Turbine Noise*, AIAA Paper 2010-645, Rome (Italy).

[8] Bortolotti, P., Branlard, E., Platt, A., Moriarty, P., Sucameli, C., and Bottasso, C. L. (2020). Aeroacoustics Noise Model of OpenFAST. Technical report, NREL, Boulder, USA. Available at: https://www.osti.gov/servlets/purl/1660130.

[9] Bortolotti, P., Guo, Y., Simley, E., Roadman, J., Hamilton, N., Moriartya, P. J., Sucameli, C. R., and Bertagnolio, F. (2021). Validation Efforts of an Open-Source Aeroacoustics Model for Wind Turbines: Preprint. Technical report, NREL, Boulder, USA. Available at: https://www.osti.gov/servlets/purl/1808274.

[10] Brooks, T. F., Pope, S. D., and Marcolini, M. A. (1989). Airfoil Self-Noise and Prediction. NASA Reference Publication 1218, Retrieved from: https://ntrs.nasa.gov/archive/nasa/casi.ntrs.nasa.gov/19890016302.pdf, NASA Langley Research Center, Hampton (VA). (Accessed: 2020-04-08).

[11] Casalino, D., Grande, E., Romani, G., Ragni, D., and Avallone, F. (2021). Definition of a benchmark for low reynolds number propeller aeroacoustics. *Aerospace Science and Technology*, 113.

[12] Casalino, D., Van der Velden, W., and Romani, G. (2022). A framework for multi-fidelity wind-turbine aeroacoustic simulations. In *28th AIAA/CEAS Aeroacoustics Conference, June 2022, Southampton, UK*.

[13] Drela, M. (1989). *XFOIL: An Analysis and Design System for Low Reynolds Number Airfoils. In: Mueller T.J. (eds) Low Reynolds Number Aerodynamics. Lecture Notes in Engineering, vol 54*. Springer, Berlin, Heidelberg.

[14] Drela, M. and Giles, M. B. (1987). Viscous-inviscid analysis of transonic and low reynolds number airfoils. *AIAA Journal*, 25(10):1347–1355.

[15] Ewert, R. (2018). RPM - the fast Random Particle-Mesh method to realize unsteady turbulent sound sources and velocity fields for CAA applications. In 13^{th} *AIAA/CEAS Aeroacoustics Conference*, Conf. Proceedings, Rome, Italy. AIAA 2007-3506.

[16] Faßmann, B., Reiche, N., Ewert, R., Herr, M., and Delfs, J. (2018). Evaluation of Wind Turbine Noise based on Numerical Simulation Methods. In 18^{th} *AIAA/CEAS Aeroacoustics Conf. (Proc.)*, Atlanta, Georgia. AIAA 2018-3924.

[17] Fischer, A., Bertagnolio, F., and Madsen, H. A. (2017). Improvement of TNO type trailing edge noise models. *European Journal of Mechanics B - Fluids*, 61:255–262.

[18] Glauert, H. (1935). *Airplane Propellers*, volume In: Aerodynamic Theory Volume IV (W. F. Durand, Ed.). Springer, Berlin, Heidelberg.

[19] Hamilton, N., Bortolotti, P. E., Jager, D., Guo, Y., Roadman, J. M., and Simley, E. (2021). Aeroacoustic Assessment of Wind Plant Controls. Technical report, NREL, Boulder, USA. Available at: https://www.osti.gov/servlets/purl/1785330.

[20] Herr, M., Ewert, R., Rautmann, C., Kamruzzaman, M., Bekiropoulos, D., Iob, A., Arina, R., Batten, P., Chakravarthy, S., and Bertagnolio, F. (2015). Broadband Trailing-Edge Noise Predictions - Overview of BANC-III Results. In 21^{th} *AIAA/CEAS Aeroacoustics Conf. (Proc.)*, AIAA Paper 2015-2847, Dallas (TX).

[21] Herr, M., Kamruzzaman, M., and Bahr, C. (2016). BANC-IV-1: TBL-Trailing-edge noise. In *Fourth Workshop on Benchmark Problems for Airframe Noise Computations (BANC-IV)*, 22^{nd} AIAA-CEAS Aeroacoustics Conference (Workshop), Lyon, France.

[22] Hornung, C., Lutz, T., and Krämer, E. (2019). A model to include turbulence-turbulence interaction in the prediction of trailing edge far field noise for high angles of attack or slightly separated flow. *Renewable Energy*, 136:945–954.

[23] Hornung, C., Scheit, C., Noffke, N., and Kamruzzamann, M. (2021). Turbulence Inflow Noise Prediction of Wind Turbine Rotors: The physically correct Representations of the Simplified Amiet and Lowson Model. In *WTN 2021*, Remote from Europe.

[24] IEC (2012). International Standard, Wind Turbines - Part 11: Acoustic Noise Measurement Techniques. IEC 61400-11, International Electrotechnical Commission, Geneva (CH). ISBN 978-2-83220-463-4.

[25] Kamruzzaman, M., Bekiropoulos, D., Lutz, T., Würz, W., and Krämer, E. (2015). A semi-empirical surface pressure spectrum model for airfoil trailing- edge noise prediction. *International Journal of Aeroacoustics*, 14(5-6):833–882.

[26] Klein, L., Gude, J., Wenz, F., Lutz, T., and Krämer, E. (2018). Advanced CFD-MBS coupling to Assess Low-Frequency Emissions from Wind Turbines. *Wind Energy Science*, 3:713–728.

[27] Larsen, T. J. and Hansen, A. M. (2007). How 2 HAWC2, The User's Manual. Tech. Rep. RISØ-R-1597(ver.3-1), Risø-DTU, Roskilde, Denmark. Available at `http://www.hawc2.dkdownload/hawc2-manual` (Accessed: 2021-03-11).

[28] Lindenburg, C. (2002). Bladmode, program for rotor blade mode analysis. Tech. Rep. ECN-C-02-050-r2, ECN, The Netherlands.

[29] Lowson, M. V. (1993). Assessment and prediction of wind turbine noise. ETSU W/13/00284/REP, UK.

[30] Lowson, M. V. and Ollerhead, J. B. (1969). A Theoretical Study of Helicopter Rotor Noise. *J. Sound Vib.*, 9(2):197–222.

[31] Madsen, H. A., Bak, C., Paulsen, U. S., Gaunaa, M., Fuglsang, P., Romblad, J., Olesen, N. A., Enevoldsen, P., Laursen, J., and Jensen, L. (2010). The DAN-AERO MW Experiments. In 48^{th} *AIAA Aerospace Sciences Meeting Including The New Horizons Forum and Aerospace Exposition (Proceedings)*, AIAA Paper 2010-645, Orlando (FL).

[32] Madsen, H. A., Larsen, T. J., Pirrung, G. R., Li, A., and Zahle, F. (2020). Implementation of the blade element momentum model on a polar grid and its aeroelastic load impact. *Wind Energy Science*, 5(1):1–27. doi:10.5194/wes-5-1-2020.

[33] Montgomerie, B., Brand, A., Bosschers, J., and van Rooij, R. (1997). Three-dimensional effects in stall. Tech. Rep. ECN-C-96-079, ECN, The Netherlands.

[34] Moriarty, P., Guidati, G., and Migliore, P. (2005). Prediction of Turbulent Inflow and Trailing-Edge Noise for Wind Turbines. In *Proc. of the* 11^{th} *AIAA/CEAS Aeroacoustics Conf.*, AIAA Paper 2005-2881, Monterey, CA.

[35] Oerlemans, S., Sijtsma, P., and López, B. M. (2007). Location and Quantification of Noise on a Wind Turbine. *J. Sound Vib.*, 299(5-6):869–883.

[36] Parchen, R. (1998). Progress report DRAW: A Prediction Scheme for Trailing-Edge Noise Based on Detailed Boundary-Layer Characteristics. TNO Rept. HAG-RPT-980023, TNO Institute of Applied Physics, The Netherlands.

[37] Paterson, R. W. and Amiet, R. K. (1976). Acoustic Radiation and Surface Pressure Characteristics of an Airfoil Due to Incident Turbulence. In 3^{rd} *AIAA Aero-Acoustics Conference*, Conf. Proceedings, Palo Alto, CA.

[38] Paterson, R. W. and Amiet, R. K. (1977). Noise and Surface Pressure Response of an Airfoil to Incident Turbulence. *Journal of Aircraft*, 14(8):729–736.

[39] Rautmann, C. (2017). Numerical Simulation Concept for Low-Noise Wind Turbine Rotors. DLR Forschungsbericht FB-2017-35, DLR (Institute for Aerodynamics and Flow Technology), Brauschweig, Germany. Dissertation.

[40] Schlinker, R. H. and Amiet, R. K. (1981). Helicopter rotor trailing edge noise.Technical Report 1. NASA Contractor Report 3470, Retrieved from: https://ntrs.nasa.gov/archive/nasa/casi.ntrs.nasa.gov/19820003986.pdf, NASA Langley Research Center. (Accessed: 2020-04-08).

[41] Sucameli, C. R., Bortolotti, P., Croce, A., and Bottasso, C. L. (2018). Comparison of some wind turbine noise emission models coupled to BEM aerodynamics. *Journal of Physics: Conference Series*, 1037:022038.

[42] van der Velden, W. C., Casalino, D., and Romani, G. (2023). Full-Scale Serrated Wind Turbine Trailing Edge Noise Certification Analysis Based on the Lattice-Boltzmann Method. In *AIAA SCITECH 2023 Forum (Proceedings)*, AIAA 2023-0970, National Harbor (MD).